Energy efficiency of underwater robots

E. Kelasidi * **K. Y. Pettersen** * **J. T. Gravdahl** **

* *Centre for Autonomous Marine Operations and Systems, Dept. of Engineering Cybernetics at NTNU, NO-7491 Trondheim, Norway, (e-mail: Eleni.Kelasidi@itk.ntnu.no, Kristin.Y.Pettersen@itk.ntnu.no).*
** *Dept. of Engineering Cybernetics at NTNU, NO-7491 Trondheim, Norway, (e-mail: Tommy.Gravdahl@itk.ntnu.no).*

Abstract: Increasing efficiency by improving locomotion methods is a key issue for underwater robots. In this paper, we investigate the power consumption of different underwater robotic systems and compare the energy efficiency of the different robots depending on the desired motion. In particular, we compare the energy efficiency of underwater snake robots, which can provide both inspection and intervention capabilities and thus are interesting candidates for the next generation inspection and intervention AUVs, with those of the widely used robots for subsea operations which are the remotely operated vehicles (ROVs). In order to compare the energy efficiency of underwater snake robots with the energy efficiency of the ROVs, a simulation study is performed comparing the total energy consumption and the cost of transportation of underwater snake robots and ROVs. The simulation results show that with respect to the cost of transportation metric and the total energy consumption the underwater snake robots are more energy efficient for all the compared motion modes compared to the ROVs.

Keywords: Underwater snake robots, energy consumption, energy efficiency of swimming robots.

1. INTRODUCTION

The use of underwater vehicles has rapidly increased the last decades since these systems are able to operate in deep and high risk areas which humans can not reach. Nowadays, autonomous underwater vehicles (AUVs) and remotely operated vehicles (ROVs) are widely used in the subsea environment for different challenging tasks (Fossen, 2011). These vehicles are suitable for various work assignments such as inspection, surveillance, maintenance, repairing equipment, building structures, and data collection, and they are extensively used in the subsea oil and gas industry and by the science community. For the long term autonomy of these systems, energy efficiency is one of the main challenges.

As has been noted in the bio-robotics community, underwater swimming robots bring a promising prospective to improve the efficiency and maneuverability of next generation underwater vehicles (Kelasidi et al., 2014b). They have several promising applications for underwater exploration, monitoring, surveillance and inspection, and they carry a lot of potential for inspection of subsea oil and gas installations. Also, for the biology and marine archeology communities, snake robots that are able to swim smoothly without much noise, and that can navigate in difficult environments such as ship wrecks, are very interesting (Kelasidi et al., 2014b). To realize operational snake robots for such underwater applications, a number of different control design challenges must first be solved. An important control problem concerns the ability to achieve efficient motion with preferably a minimum amount of consumed energy in order to be able to undertake longer missions, and this is the topic of this paper.

⋆ This work was partly supported by the Research Council of Norway through project no. 205622 and its Centres of Excellence funding scheme, project no. 223254-AMOS.

Studies of hyper-redundant mechanisms (HRMs) have largely restricted themselves to land-based studies, where several models for snake robots have been proposed (Liljebäck et al., 2013). Empirical and analytic studies of snake locomotion were reported by Gray (1933), while the work of Hirose (1993) is among the first attempts to develop a snake robot prototype. Comparing amphibious snake robots to the traditional land-based ones, the former have the advantage of adaptability to aquatic environments. In Kelasidi et al. (2014b), the authors propose a model of underwater snake robots, where the dynamic equations are written in closed form. This modeling approach takes into account both the linear and the nonlinear drag forces (resistive fluid forces), the added mass effect (reactive fluid forces), the fluid moments and the current effects. Compared to other models (Boyer et al., 2006; Chen et al., 2011; Wiens and Nahon, 2012; Khalil et al., 2007), it is an advantage from an analysis point of view that the model is in closed form, as opposed to including numerical evaluations of the drag effects. In addition, it is beneficial that it includes both resistive and reactive fluid forces, since swimming snake robots operate at Reynolds numbers that require both these effects to be taken into account. Therefore, the analysis in this paper will be based on the dynamic model presented in Kelasidi et al. (2014b).

In Kelasidi et al. (2015), the relationships between the parameters of the gait patterns, the consumed energy and the forward velocity for different motion patterns for underwater snake robots were investigated. In addition, empirical rules were proposed in order to choose the most efficient motion pattern. In this paper, we present simulation results in order to compare the power consumption of swimming snake robots with that of today's benchmark solution for subsea inspection, maintenance and repair, which are ROVs, and comparison results are thus obtained for the power consumption of underwater snake

robots and ROVs. This paper presents results by investigating the power consumption of different underwater robotic systems and pointing out the most efficient vehicle depending on the desired motion. The purpose of this study is to investigate the issues that could influence both the motion performance and the transportation performance of underwater snake robots and ROVs. In particular, the energy index (Shi et al., 2008), is used in order to compare the energy efficiency of underwater snake robots compared with the widely used remotely operated vehicles. A similar approach is used in order study the energy index of different transformation modes for ships in Shi et al. (2008). Comparison results are obtained for the total energy consumption and the cost of transportation of underwater snake robots and ROVs. The simulation results show that, with respect to the cost of transportation metric and the total consumed energy the underwater snake robots are more energy efficient for all the compared motion modes. To the authors' best knowledge, a comparison of the consumed energy between underwater swimming snake robots and remotely operated vehicles have not been investigated in previous literature.

The paper is organized as follows. Section II presents the dynamic model and the motion pattern of an underwater snake robot, while the kinematics and the dynamics of remotely operated vehicles are outlined in Section III. The energetics of underwater snake robots and ROVs are presented in Section IV, followed by simulation results for both underwater snake robots and ROVs in Section V. Finally, conclusions and suggestions for further research are given in Section VI.

2. UNDERWATER SNAKE ROBOTS

This section briefly presents a model of the kinematics and dynamics of an underwater snake robot moving in a virtual horizontal plane. A more detailed presentation of the model can be found in Kelasidi et al. (2014b). In addition, a general sinusoidal motion pattern proposed in Kelasidi et al. (2014a) will be presented, and also a low-level joint controller is presented.

2.1 Notations and defined symbols

The underwater snake robot consists of n rigid links of equal length $2l$ interconnected by $n-1$ joints. The links are assumed to have the same mass m and moment of inertia $J = \frac{1}{3}ml^2$. The mass of each link is uniformly distributed so that the link CM (center of mass) is located at its center point (at length l from the joint at each side). The total mass of the snake robot is therefore nm. In the following sections, the kinematics and dynamics of the robot will be described in terms of the mathematical symbols described in Table 1 and illustrated in Fig. 1. The following vectors and matrices are used in the subsequent sections:

$$\mathbf{A} = \begin{bmatrix} 1 & 1 & & \\ & \ddots & \ddots & \\ & & 1 & 1 \end{bmatrix}, \ \mathbf{D} = \begin{bmatrix} 1 & -1 & & \\ & \ddots & \ddots & \\ & & 1 & -1 \end{bmatrix},$$

where $\mathbf{A}, \mathbf{D} \in \mathbb{R}^{(n-1)\times n}$. Furthermore,

$$\mathbf{e} = \begin{bmatrix} 1 & \dots & 1 \end{bmatrix}^T \in \mathbb{R}^n, \ \mathbf{E} = \begin{bmatrix} \mathbf{e} & \mathbf{0}_{n\times 1} \\ \mathbf{0}_{n\times 1} & \mathbf{e} \end{bmatrix} \in \mathbb{R}^{2n\times 2},$$

$$\mathbf{S}_\theta = \text{diag}(\sin\boldsymbol{\theta}) \in \mathbb{R}^{n\times n}, \qquad \mathbf{C}_\theta = \text{diag}(\cos\boldsymbol{\theta}) \in \mathbb{R}^{n\times n}$$

$$\dot{\boldsymbol{\theta}}^2 = \begin{bmatrix} \dot{\theta_1}^2 & \dots & \dot{\theta_n}^2 \end{bmatrix}^T \in \mathbb{R}^n, \ \mathbf{J} = J\mathbf{I}_n, \mathbf{K} = \mathbf{A}^T \left(\mathbf{D}\mathbf{D}^T\right)^{-1} \mathbf{D}$$

2.2 Kinematics of the underwater snake robot

The snake robot is assumed to move in a virtual horizontal plane, fully immersed in water, and has n+2 degrees of freedom

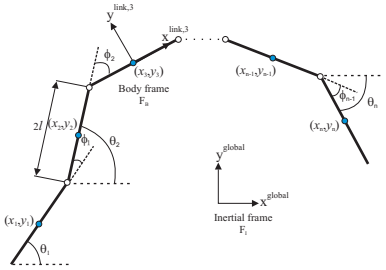

(a) Kinematic parameters

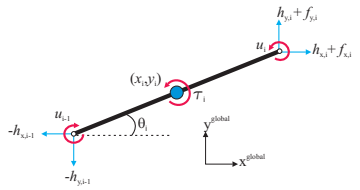

(b) Forces and torques acting on each link

Fig. 1. Underwater snake robot

Table 1. Definition of mathematical terms

Symbol	Description	Vector
n	The number of links	
l	The half length of a link	
m	Mass of each link	
J	Moment of inertia of each link	
θ_i	Angle between link i and the global x axis	$\boldsymbol{\theta} \in \mathbb{R}^n$
ϕ_i	Angle of joint i	$\boldsymbol{\phi} \in \mathbb{R}^{n-1}$
(x_i, y_i)	Global coordinates of the CM of link i	$\mathbf{X}$,$\mathbf{Y} \in \mathbb{R}^n$
(p_x, p_y)	Global coordinates of the CM of the robot	$\mathbf{p}_{CM} \in \mathbb{R}^2$
u_i	Actuator torque of joint between link i and link $i+1$	$\mathbf{u} \in \mathbb{R}^{n-1}$
u_{i-1}	Actuator torque of joint between link i and link $i-1$	$\mathbf{u} \in \mathbb{R}^{n-1}$
$(f_{x,i}, f_{y,i})$	Fluid force on link i	$\mathbf{f}_x$,$\mathbf{f}_y \in \mathbb{R}^n$
τ_i	Fluid torque on link i	$\boldsymbol{\tau} \in \mathbb{R}^n$
$(h_{x,i}, h_{y,i})$	Joint constraint force on link i from link $i+1$	$\mathbf{h}_x$,$\mathbf{h}_y \in \mathbb{R}^{n-1}$
$-(h_{x,i-1}, h_{y,i-1})$	Joint constraint force on link i from link $i-1$	$\mathbf{h}_x$,$\mathbf{h}_y \in \mathbb{R}^{n-1}$

(n links angles and the x-y position of the robot). The *link angle* of each link $i \in 1, \dots, n$ of the snake robot is denoted by $\theta_i \in \mathbb{R}$, while the *joint angle* of joint $i \in 1, \dots, n-1$ is given by $\phi_i = \theta_i - \theta_{i-1}$. The *heading* (or *orientation*) $\bar{\theta} \in \mathbb{R}$ of the snake is defined as the average of the link angles, i.e. as (Liljebäck et al., 2013)

$$\bar{\theta} = \frac{1}{n}\sum_{i=1}^{n} \theta_i. \tag{1}$$

The global frame position $\mathbf{p}_{\text{CM}} \in \mathbb{R}^2$ of the CM (center of mass) of the robot is given by

$$\mathbf{p}_{\text{CM}} = \begin{bmatrix} p_x \\ p_y \end{bmatrix} = \begin{bmatrix} \frac{1}{nm}\sum_{i=1}^{n} m x_i \\ \frac{1}{nm}\sum_{i=1}^{n} m y_i \end{bmatrix} = \frac{1}{n}\begin{bmatrix} \mathbf{e}^T\mathbf{X} \\ \mathbf{e}^T\mathbf{Y} \end{bmatrix}, \tag{2}$$

where (x_i, y_i) are the global frame coordinates of the CM of link i, $\mathbf{X}$= $\begin{bmatrix} x_1, \dots, x_n \end{bmatrix}^T \in \mathbb{R}^n$ and $\mathbf{Y}$= $\begin{bmatrix} y_1, \dots, y_n \end{bmatrix}^T \in \mathbb{R}^n$. The forward velocity of the robot is denoted by $\bar{v}_t \in \mathbb{R}$ and is defined as the component of the CM velocity along the current heading of the snake, i.e.

$$\bar{v}_t = \dot{p}_x \cos\bar{\theta} + \dot{p}_y \sin\bar{\theta}. \tag{3}$$

2.3 Hydrodynamic modeling

As has been noted in the bio-robotics community, underwater snake (eel-like) robots bring a promising prospective to improve the efficiency and maneuverability of next generation underwater vehicles. The dynamic modeling of the contact forces is, however, quite complicated compared to the modeling of the overall rigid motion. In Kelasidi et al. (2014b) it is shown that the fluid forces on all links can be expressed in vector form as

$$\mathbf{f} = \begin{bmatrix} \mathbf{f_x} \\ \mathbf{f_y} \end{bmatrix} = \begin{bmatrix} \mathbf{f_{A_x}} \\ \mathbf{f_{A_y}} \end{bmatrix} + \begin{bmatrix} \mathbf{f}^{\,\mathrm{I}}_{\mathbf{D_x}} \\ \mathbf{f}^{\,\mathrm{I}}_{\mathbf{D_y}} \end{bmatrix} + \begin{bmatrix} \mathbf{f}^{\,\mathrm{II}}_{\mathbf{D_x}} \\ \mathbf{f}^{\,\mathrm{II}}_{\mathbf{D_y}} \end{bmatrix}. \tag{4}$$

The vectors $\mathbf{f_{A_x}}$ and $\mathbf{f_{A_y}}$ represent the effects from added mass forces and are expressed as

$$\begin{aligned} \begin{bmatrix} \mathbf{f_{A_x}} \\ \mathbf{f_{A_y}} \end{bmatrix} = &- \begin{bmatrix} \mu_n (\mathbf{S}_\theta)^2 & -\mu_n \mathbf{S}_\theta \mathbf{C}_\theta \\ -\mu_n \mathbf{S}_\theta \mathbf{C}_\theta & \mu_n (\mathbf{C}_\theta)^2 \end{bmatrix} \begin{bmatrix} \ddot{\mathbf{X}} \\ \ddot{\mathbf{Y}} \end{bmatrix} \\ &- \begin{bmatrix} -\mu_n \mathbf{S}_\theta \mathbf{C}_\theta & -\mu_n (\mathbf{S}_\theta)^2 \\ \mu_n (\mathbf{C}_\theta)^2 & \mu_n \mathbf{S}_\theta \mathbf{C}_\theta \end{bmatrix} \begin{bmatrix} \mathbf{V}_x^a \\ \mathbf{V}_y^a \end{bmatrix} \dot{\boldsymbol{\theta}}, \end{aligned} \tag{5}$$

where $\mathbf{V}_x^a = \mathrm{diag}\,(V_{x,1}, \ldots, V_{x,n}) \in \mathbb{R}^{n \times n}$, $\mathbf{V}_y^a = \mathrm{diag}\,(V_{y,1}, \ldots, V_{y,n}) \in \mathbb{R}^{n \times n}$ and $[V_{x,i}, V_{y,i}]^T$ is the current velocity expressed in inertial frame coordinates. The vectors $\mathbf{f}^{\,\mathrm{I}}_{\mathbf{D_x}}$, $\mathbf{f}^{\,\mathrm{I}}_{\mathbf{D_y}}$ and $\mathbf{f}^{\,\mathrm{II}}_{\mathbf{D_x}}$, $\mathbf{f}^{\,\mathrm{II}}_{\mathbf{D_y}}$ present the effects from the linear (6) and nonlinear drag forces (7), respectively, where the relative velocities are given by (8).

$$\begin{bmatrix} \mathbf{f}^{\,\mathrm{I}}_{\mathbf{D_x}} \\ \mathbf{f}^{\,\mathrm{I}}_{\mathbf{D_y}} \end{bmatrix} = - \begin{bmatrix} c_t (\mathbf{C}_\theta)^2 + c_n (\mathbf{S}_\theta)^2 & (c_t - c_n) \mathbf{S}_\theta \mathbf{C}_\theta \\ (c_t - c_n) \mathbf{S}_\theta \mathbf{C}_\theta & c_t (\mathbf{S}_\theta)^2 + c_n (\mathbf{C}_\theta)^2 \end{bmatrix} \begin{bmatrix} \dot{\mathbf{X}} - \mathbf{V}_x \\ \dot{\mathbf{Y}} - \mathbf{V}_y \end{bmatrix} \tag{6}$$

$$\begin{bmatrix} \mathbf{f}^{\,\mathrm{II}}_{\mathbf{D_x}} \\ \mathbf{f}^{\,\mathrm{II}}_{\mathbf{D_y}} \end{bmatrix} = - \begin{bmatrix} c_t \mathbf{C}_\theta & -c_n \mathbf{S}_\theta \\ c_t \mathbf{S}_\theta & c_n \mathbf{C}_\theta \end{bmatrix} \mathrm{sgn} \left(\begin{bmatrix} \mathbf{V_{r_x}} \\ \mathbf{V_{r_y}} \end{bmatrix} \right) \begin{bmatrix} \mathbf{V_{r_x}}^2 \\ \mathbf{V_{r_y}}^2 \end{bmatrix} \tag{7}$$

$$\begin{bmatrix} \mathbf{V_{r_x}} \\ \mathbf{V_{r_y}} \end{bmatrix} = \begin{bmatrix} \mathbf{C}_\theta & \mathbf{S}_\theta \\ -\mathbf{S}_\theta & \mathbf{C}_\theta \end{bmatrix} \begin{bmatrix} \dot{\mathbf{X}} - \mathbf{V}_x \\ \dot{\mathbf{Y}} - \mathbf{V}_y \end{bmatrix} \tag{8}$$

In addition, the fluid torques on all links are

$$\boldsymbol{\tau} = -\boldsymbol{\Lambda}_1 \ddot{\boldsymbol{\theta}} - \boldsymbol{\Lambda}_2 \dot{\boldsymbol{\theta}} - \boldsymbol{\Lambda}_3 \dot{\boldsymbol{\theta}} |\dot{\boldsymbol{\theta}}|, \tag{9}$$

where $\boldsymbol{\Lambda}_1 = \lambda_1 \mathbf{I}_n$, $\boldsymbol{\Lambda}_2 = \lambda_2 \mathbf{I}_n$ and $\boldsymbol{\Lambda}_3 = \lambda_3 \mathbf{I}_n$. The coefficients c_t, c_n, λ_2, λ_3 represent the drag forces parameters due to the pressure difference between the two sides of the body, and the parameters μ_n, λ_1 represent the added mass of the fluid carried by the moving body.

2.4 Equations of motion

This section presents the equations of motion for the underwater snake robot. In Kelasidi et al. (2014b), it is shown that the acceleration of the CM may be expressed as

$$\begin{aligned} \begin{bmatrix} \ddot{p}_x \\ \ddot{p}_y \end{bmatrix} = &-\mathbf{M}_p \begin{bmatrix} \mathbf{e}^T \mu_n \mathbf{S}_\theta^2 & -\mathbf{e}^T \mu_n \mathbf{S}_\theta \mathbf{C}_\theta \\ -\mathbf{e}^T \mu_n \mathbf{S}_\theta \mathbf{C}_\theta & \mathbf{e}^T \mu_n \mathbf{C}_\theta^2 \end{bmatrix} \begin{bmatrix} l\mathbf{K}^T (\mathbf{C}_\theta \dot{\boldsymbol{\theta}}^2 + \mathbf{S}_\theta \ddot{\boldsymbol{\theta}}) \\ l\mathbf{K}^T (\mathbf{S}_\theta \dot{\boldsymbol{\theta}}^2 - \mathbf{C}_\theta \ddot{\boldsymbol{\theta}}) \end{bmatrix} \\ &- \mathbf{M}_p \begin{bmatrix} -\mathbf{e}^T \mu_n \mathbf{S}_\theta \mathbf{C}_\theta & -\mathbf{e}^T \mu_n \mathbf{S}_\theta^2 \\ \mathbf{e}^T \mu_n \mathbf{C}_\theta^2 & \mathbf{e}^T \mu_n \mathbf{S}_\theta \mathbf{C}_\theta \end{bmatrix} \begin{bmatrix} \mathbf{V}_x^a \\ \mathbf{V}_y^a \end{bmatrix} \dot{\boldsymbol{\theta}} + \mathbf{M}_p \begin{bmatrix} \mathbf{e}^T \mathbf{f_{Dx}} \\ \mathbf{e}^T \mathbf{f_{Dy}} \end{bmatrix} \end{aligned} \tag{10}$$

where

$$\mathbf{M}_p = \begin{bmatrix} m_{11} & m_{12} \\ m_{21} & m_{22} \end{bmatrix} = \begin{bmatrix} nm + \mathbf{e}^T \mu_n \mathbf{S}_\theta^2 \mathbf{e} & -\mathbf{e}^T \mu_n \mathbf{S}_\theta \mathbf{C}_\theta \mathbf{e} \\ -\mathbf{e}^T \mu_n \mathbf{S}_\theta \mathbf{C}_\theta \mathbf{e} & nm + \mathbf{e}^T \mu_n \mathbf{C}_\theta^2 \mathbf{e} \end{bmatrix}^{-1}. \tag{11}$$

and $\mathbf{f_{Dx}} = \mathbf{f}^{\,\mathrm{I}}_{\mathbf{D_x}} + \mathbf{f}^{\,\mathrm{II}}_{\mathbf{D_x}}$ and $\mathbf{f_{Dy}} = \mathbf{f}^{\,\mathrm{I}}_{\mathbf{D_y}} + \mathbf{f}^{\,\mathrm{II}}_{\mathbf{D_y}}$ are the drag forces in x and y directions. In addition, it is shown in Kelasidi et al. (2014b) that the model of an underwater snake robot may be expressed as

$$\mathbf{M}_{\boldsymbol{\theta}} \ddot{\boldsymbol{\theta}} + \mathbf{W}_{\boldsymbol{\theta}} \dot{\boldsymbol{\theta}}^2 + \mathbf{V}_\theta \dot{\boldsymbol{\theta}} + \boldsymbol{\Lambda}_3 |\dot{\boldsymbol{\theta}}| \dot{\boldsymbol{\theta}} + \mathbf{K_{Dx}} \mathbf{f_{Dx}} + \mathbf{K_{Dy}} \mathbf{f_{Dy}} = \mathbf{D}^T \mathbf{u}, \tag{12}$$

where $\mathbf{M}_\theta$, $\mathbf{W}_\theta$, $\mathbf{V}_\theta$, $\mathbf{K_{Dx}}$ and $\mathbf{K_{Dy}}$ are defined as

$$\begin{aligned} \mathbf{M}_\theta = &\mathbf{J} + ml^2 \mathbf{S}_\theta \mathbf{V} \mathbf{S}_\theta + ml^2 \mathbf{C}_\theta \mathbf{V} \mathbf{C}_\theta + \\ &\boldsymbol{\Lambda}_1 + l^2 \mu_n \mathbf{K}_1 \mathbf{K}^T \mathbf{S}_\theta + l^2 \mu_n \mathbf{K}_2 \mathbf{K}^T \mathbf{C}_\theta \end{aligned} \tag{13}$$

$$\mathbf{W}_\theta = ml^2 \mathbf{S}_\theta \mathbf{V} \mathbf{C}_\theta - ml^2 \mathbf{C}_\theta \mathbf{V} \mathbf{S}_\theta + l^2 \mu_n \mathbf{K}_1 \mathbf{K}^T \mathbf{C}_\theta - l^2 \mu_n \mathbf{K}_2 \mathbf{K}^T \mathbf{S}_\theta \tag{14}$$

$$\mathbf{V}_\theta = \boldsymbol{\Lambda}_2 - l\mu_n \mathbf{K}_2 \mathbf{V}_x^a - l\mu_n \mathbf{K}_1 \mathbf{V}_y^a \tag{15}$$

$$\mathbf{K_{Dx}} = l\mu_n m_{11} A_1 \mathbf{e}\mathbf{e}^T - l\mu_n m_{21} A_2 \mathbf{e}\mathbf{e}^T - l\mathbf{S}_\theta \mathbf{K} \tag{16}$$

$$\mathbf{K_{Dy}} = l\mu_n m_{12} A_1 \mathbf{e}\mathbf{e}^T - l\mu_n m_{22} A_2 \mathbf{e}\mathbf{e}^T + l\mathbf{C}_\theta \mathbf{K} \tag{17}$$

where $\mathbf{K}_1 = \mathbf{A}_1 + \mu_n \mathbf{A}_1 \mathbf{e}\mathbf{e}^T (m_{12} \mathbf{S}_\theta \mathbf{C}_\theta - m_{11} \mathbf{S}_\theta^2) - \mu_n \mathbf{A}_2 \mathbf{e}\mathbf{e}^T (m_{22} \mathbf{S}_\theta \mathbf{C}_\theta - m_{21} \mathbf{S}_\theta^2)$, $\mathbf{K}_2 = \mathbf{A}_2 - \mu_n \mathbf{A}_1 \mathbf{e}\mathbf{e}^T (m_{11} \mathbf{S}_\theta \mathbf{C}_\theta - m_{12} \mathbf{C}_\theta^2) + \mu_n \mathbf{A}_2 \mathbf{e}\mathbf{e}^T (m_{21} \mathbf{S}_\theta \mathbf{C}_\theta - m_{22} \mathbf{C}_\theta^2)$, $\mathbf{A}_1 = \mathbf{S}_\theta \mathbf{K} \mathbf{S}_\theta^2 + \mathbf{C}_\theta \mathbf{K} \mathbf{S}_\theta \mathbf{C}_\theta$ and $\mathbf{A}_2 = \mathbf{S}_\theta \mathbf{K} \mathbf{S}_\theta \mathbf{C}_\theta + \mathbf{C}_\theta \mathbf{K} \mathbf{C}_\theta^2$.

In summary, the equations of motion for the underwater snake robot are given by (10) and (12). By introducing the state variable $\mathbf{x} = \left[\boldsymbol{\theta}^T, \mathbf{p}_{CM}^T, \dot{\boldsymbol{\theta}}^T, \dot{\mathbf{p}}_{CM}^T \right]^T \in \mathbb{R}^{2n+4}$, we can rewrite the model of the robot compactly in state space form as

$$\dot{\mathbf{x}} = \left[\dot{\boldsymbol{\theta}}^T, \dot{\mathbf{p}}_{CM}^T, \ddot{\boldsymbol{\theta}}^T, \ddot{\mathbf{p}}_{CM}^T \right]^T = \mathbf{F}(\mathbf{x}, \mathbf{u}) \tag{18}$$

where the elements of $\mathbf{F}(\mathbf{x}, \mathbf{u})$ are found by solving (10) and (12) for $\ddot{\mathbf{p}}_{CM}$ and $\ddot{\boldsymbol{\theta}}$, respectively.

2.5 Motion Pattern

Previous studies on swimming snake robots have focused on two motion patterns; lateral undulation and eel-like motion. In this paper, we will use a general sinusoidal motion pattern that describes a broader class of motion patterns including lateral undulation and eel-like motion as special cases (Kelasidi et al., 2014a). A general sinusoidal motion pattern can be achieved by making each joint $i \in \{1, \cdots, n-1\}$ of the underwater snake robot track the sinusoidal reference signal

$$\phi_i^*(t) = \alpha \mathrm{g}(i, n) \sin(\omega t + (i-1)\delta) + \gamma, \tag{19}$$

where α and ω are the maximum amplitude and the frequency, respectively, δ determines the phase shift between the joints, while the function $\mathrm{g}(i, n)$ is a scaling function for the amplitude of joint i which allows (19) to describe a quite general class of sinusoidal functions, including several different snake motion patterns. For instance, $\mathrm{g}(i, n) = 1$ gives lateral undulation, while $\mathrm{g}(i, n) = (n - i)/(n + 1)$ gives eel-like motion. The parameter γ is a joint offset coordinate that can be used to control the direction of the locomotion (Kelasidi et al., 2014b). In particular, in Liljebäck et al. (2013) and Guo (2006), γ is shown to affect the direction of locomotion in the case of land-based snake robots and fish robots, respectively.

2.6 Low-level joint control

A PD-controller is used to calculate the joints' actuator torques from the joints' reference angles according to

$$u_i = \ddot{\phi}_i^* + K_{p,i}(\phi_i^* - \phi_i) + K_{d,i}(\dot{\phi}_i^* - \dot{\phi}_i), \quad i = 1, \ldots, n-1\,, \tag{20}$$

where $K_{p,i} > 0$ and $K_{d,i} > 0$ are the gains of the controller.

3. REMOTELY OPERATED VEHICLES (ROVS)

This section briefly presents a model of the kinematics and dynamics of a remotely operated vehicle (ROV). A more detailed presentation of the model can be found in Fossen (2011).

The dynamics of ROVs are highly nonlinear due to the coupling of the rigid body dynamics and the hydrodynamic forces on the vehicle. The equation of motion of a remotely operated vehicle can be written as:

$$\mathbf{M}_{\mathrm{r}} \ddot{\mathbf{q}} + \mathbf{C}_{\mathrm{r}}(\dot{\mathbf{q}}) \dot{\mathbf{q}} + \mathbf{D}_{\mathrm{r}}(\dot{\mathbf{q}}) \dot{\mathbf{q}} + g(\mathbf{x}_{\mathrm{r}}) = \boldsymbol{\tau}_{\mathrm{r}} \tag{21}$$

$$\dot{\mathbf{x}}_{\mathrm{r}} = \mathbf{J}_r(\mathbf{x}_{\mathrm{r}}) \dot{\mathbf{q}} \tag{22}$$

where $\boldsymbol{\tau}_{\mathrm{r}} \in \mathbb{R}^k$ is the vector of control forces and moments, $\mathbf{q} \in \mathbb{R}^k$ is a vector of virtual coordinates and $\dot{\mathbf{q}} = [u_r, \nu_r, w_r, p_r, q_r, r_r]^T$ is the body-fixed linear and angular velocity vector. The earth-fixed position and angle vector is defined as $\mathbf{x}_{\mathrm{r}} = [x_r, y_r, z_r, \phi_r, \theta_r, \psi_r]^T \in \mathbb{R}^k$. $\mathbf{M}_{\mathrm{r}}$ is a $k \times k$ system inertia matrix, $\mathbf{C}_{\mathrm{r}}(\dot{\mathbf{q}})$ is a $k \times k$ matrix of centrifugal and Coriolis terms, $\mathbf{D}_{\mathrm{r}}(\dot{\mathbf{q}})$ is a $k \times k$ matrix of hydrodynamic damping terms, $g(\mathbf{x}_{\mathrm{r}})$ is a $k \times 1$ vector including restoring forces and moments and $\mathbf{J}_r(\mathbf{x}_{\mathrm{r}})$ is a $k \times k$ kinematic transformation matrix, which is a function of the angles ϕ_r, θ_r, ψ_r. A more detailed presentation of these terms are given in Fossen (2011).

4. ENERGY CONSUMPTION

In this section, we will present the energy consumption analysis approach that is applied for both underwater snake robots and remotely operated vehicles. In addition, we will present a cost of transportation metric that makes it possible to obtain comparison results of the consumed energy for different systems.

4.1 Energetics of underwater snake robots

For underwater snake robots, the propulsion is generated by the motion of the joints and its interaction with the surrounding fluid. The actuator torque input to the joints is thus transformed into a combination of joint motion and energy that is dissipated by the fluid. We assume that we have perfect joints and thus the total amount of energy of the system (E_{s}) generated by this input is the sum of kinetic energy (E_{kinetic}) and the energy that is dissipated to the surrounding fluid (E_{fluid}) (Wiens and Nahon, 2012; Shi et al., 2008). The sum of these two is thus the total energy that is spent for the propulsion of the robot.

$$E_{\text{s}} = E_{\text{kinetic}} + E_{\text{fluid}} \tag{23}$$

where E_{s} is given by

$$E_{\text{s}} = \int_0^T \left(\sum_{i=1}^{n-1} u_i(t)\dot{\phi}_i(t) \right) dt. \tag{24}$$

T is the time that corresponds to a complete swimming cycle, u_i is the actuation torque of joint i given by (20) and $\dot{\phi}_i$ is the joint's angular velocity defined as $\dot{\phi}_i = \dot{\theta}_i - \dot{\theta}_{i-1}$.

For a complete swimming cycle, T, the averaged power consumption, P_{avg}, is calculated as follows

$$P_{\text{avg}} = \frac{1}{T} \int_0^T \left(\sum_{i=1}^{n-1} u_i(t)\dot{\phi}_i(t) \right) dt. \tag{25}$$

The underwater snake robot considered in this paper is based on the assumption that the robot is un-tethered and thus the energy consumption is crucial for achieving long term-autonomy of this system.

4.2 Energetics of remotely operated vehicles (ROVs)

Similarly to the underwater snake robots, the total amount of energy of ROVs (E_{total}) is the sum of kinetic energy (E_{kinetic}) and the energy that is dissipated to the surrounding fluid (E_{fluid}). For an ROV the power is the input to the system that is generated through the actuator forces and torques applied to the system. The total amount of the energy that is spent for the propulsion of the vehicle is given by

$$E_{\text{r}} = \int_0^{T_{\text{r}}} \boldsymbol{\tau}_{\text{r}}(t)\dot{\mathbf{q}}(t)\, dt, \tag{26}$$

where T_{r} is the a complete time to achieve a specified motion. In addition, the average power consumption for ROVs, P^r_{avg}, is given by the following expression

$$P^r_{\text{avg}} = \frac{1}{T_r} \int_0^{T_{\text{r}}} \boldsymbol{\tau}_{\text{r}}(t)\dot{\mathbf{q}}(t)\, dt. \tag{27}$$

4.3 Efficient Motion

For underwater applications, it is important to find an optimum combination of different underwater vehicles or different motion modes, which lead to the lowest energy consumption. To compare the energy consumption of different vehicles, we need a suitable basis for comparison. In this study, in order to compare vehicles with different dimensions and characteristics, a dimensionless quantity is used. Generally, the energy index/*cost of transportation* quantifies the energy efficiency of a vehicle, or of a robotic system in our case. The cost of transportation has been used in a wide range of applications in order to define the most energy efficient motion of different systems (Shi et al., 2008). In this study, the cost of transportation is defined as

$$COT = \frac{\text{Energy}}{\text{Mass} \times g \times \text{Distance}}. \tag{28}$$

Cost of transportation is non-dimensional and it quantifies how much energy that is applied to a system of a specified mass in order to move the system a defined distance (the ratio between the consumed energy and the transferred weight times the covered distance). Using the energy index approach, the vehicle is operated without taking into account the kind of propulsion system that is implemented inside. This coefficient is useful for the comparison of different types of transportation, since it gives an indication of the required (total) power to a system and the effective power. A similar approach is used in order to indicate the relationship between the mechanical index and the energy index of different transformation modes for ships in Shi et al. (2008). In particular, the purpose of the case study in Shi et al. (2008) was to investigate the issues that could influence both the moving performance and the transportation performance of ships. In this paper, we will use the energy index in order to compare the energy efficiency of underwater snake robots to the energy efficiency of the widely used remotely operated vehicles.

5. SIMULATION STUDY

In this section, simulation results will be presented for underwater snake robots and ROV reaching the distance of 4 m. In this initial study, the current effects have not been considered. The models were implemented in *Matlab R2013b*. The dynamics was calculated using the *ode23tb* solver with a relative and absolute error tolerance of 10^{-4}.

5.1 Simulation parameters for underwater snake robot

We consider snake robots with respectively $n = 5$, $n = 10$, $n = 20$ links, each one having length $2l = 2 \times 0.14$ m. The five links constitute a rather short snake robot, while ten to twenty links constitute a more normal length of snake robots. The mass of each link is $m = 0.6597$ kg and is chosen so to fulfil the neutrally buoyant assumption. The initial values of the states of the snake robot were set to initial reference values at $t = 0$ with its heading along the inertial x axis. The hydrodynamic parameters are $c_t = 0.2639$, $c_n = 8.4$, $\mu_n = 0.3958$, $\lambda_1 = 2.298810^{-7}$, $\lambda_2 = 4.310310^{-4}$ and $\lambda_3 = 2.262910^{-5}$. An extensive discussion about the values of the fluid parameters can be found in Kelasidi et al. (2014b). The joint PD controller (20) is used for each joint with parameters $k_p = 200$, $k_d = 5$, and lateral undulation and eel-like motion are achieved by choosing $\text{g}(i, n) = 1$ and $\text{g}(i, n) = (n - i)/(n + 1)$, respectively. It should be noted that the anisotropic friction

property that is needed for forward locomotion (Kelasidi et al., 2014b), is achieved by a low drag coefficient in the tangential direction and a higher one in the perpendicular. The gait pattern parameters are presented in each simulation result.

5.2 Simulation parameters for ROV

Simulation results will be presented for a fairly typical model of a ROV. The mass of the ROV is $m_r = 3184$ kg with the volume of the vehicle being $V_r = 3.2$ and the vehicle is neutrally buoyant. The location of the center of gravity (CG) and the center of buoyancy are given by $r_g = [-0.00234, 0.00301, -0.02119]^T$ and $r_b = [0.12, 0, 0.197]^T$, respectively. The mass matrix, which includes the added mass effects, is given by $\mathbf{M}_{RB} = 1.1 m_r \mathbf{I}_r$. The inertia matrix, $\mathbf{I}_r$, the system inertia matrix, $\mathbf{M}_r$, and the damping matrix, $\mathbf{D}_r$, are defined in the following vector and matrices:

$$\mathbf{I}_r = \begin{bmatrix} 1964.2 & 0 & -120 \\ 0 & 3209.2 & 7 \\ -120 & 7 & 3031.2 \end{bmatrix},$$

$$\mathbf{M}_r = \begin{bmatrix} 3502.4 & 0 & 0 & 0 & -67.5 & -9.6 \\ 0 & 3502.4 & 067.5 & 0 & -7.5 & \\ 0 & 0 & 3502.4 & 9.6 & 7.5 & 0 \\ 0 & 67.5 & 9.6 & 1964.2 & 0 & -120 \\ -67.5 & 0 & 7.5 & 0 & 3209.2 & 7 \\ -9.6 & -7.5 & 0 & -120 & 7 & 3031.2 \end{bmatrix},$$

$$\mathbf{D}_r = \text{diag}\,(1321, 2525, 2525, 192, 192, 192)\,.$$

By using the MSS toolbox in Matlab, the centrifugal and Coriolis matrix, $\mathbf{C}_{\text{r}}(\dot{\mathbf{q}})$, is calculated for the ROV model. The initial values of the states of the ROV are chosen to be $[0, 0, -2, 0, 0, 0]^T$ and the vehicle is freely moved by applying the input $\boldsymbol{\tau}_{\text{r}} = [\tau_x, 0, 0, 0, 0, 0]^T$.

5.3 Simulation results

In Fig. 2 simulation results are presented based on the model of the ROV presented in Section 5.2. The system is freely moved with τ_x taking values in the range $[2 \cdot 10^3, 8 \cdot 10^3]$ N, to reach the distance of 4 m. Using (26) and (28), the total energy consumption and the cost of transportation are calculated. The max velocities that are achieved for different values of the input torque are presented in Fig. 2a. From Fig. 2b, we can see that the maximum energy is consumed for the maximum achieved forward velocity as it was expected. From Fig. 2c, we can conclude that faster motions are not energy efficient and from a power consumption perspective, the vehicle is preferred to move the given distance of 4 m at the minimum possible velocity.

In addition, simulation results are presented in Fig. 3 - Fig. 6 for underwater snake robots of different length for both lateral undulation and eel-like motion patterns. Using (24) and (28), the total energy consumption and the cost of transportation are calculated. Fig. 3 and Fig. 5 present the total power consumption for lateral undulation and eel-like motion, respectively. In Fig. 4 and Fig. 6 the cost of transportation is presented for both lateral undulation and eel-like motion. In addition, the minimum and the maximum values of the total energy consumption and the cost of transportation are given in Table 2 - 3 for the simulation results presented in Fig. 3 - 6. From Table 2 and Table 3, we can see that the eel-like motion pattern is more energy efficient for snake robots with $n > 10$ links while lateral undulation is more energy efficient for snake robot with $n < 10$ links. In addition, we see that by increasing the number of links the total energy consumption and thus the cost of transportation are increased for both lateral undulation and eel-like motion, as were expected since by increasing the number of links n we need more $(n-1)$ servo motors for the joint actuation.

Comparing these results with the results for the ROV presented in Fig. 2, we can conclude that the underwater snake robots are more energy efficient by considering the cost of transportation as the metric. In particular, for the ROV the minimum and maximum values of the cost of transportation are 6.6743 and 1.8068, respectively, and the more energy efficient motion is achieved for the lowest velocities of the ROV. Even for the lowest velocities of the ROV the underwater snake robots are more energy efficient using COT as the metric. In addition, we see from Fig. 2b that the minimum and the maximum total energy consumption for ROV to move the 4 m distance are $2.2574 \cdot 10^5$ and $8.3389 \cdot 10^5$ Joule, respectively. Comparing this result with the total energy consumption of the underwater snake robots presented in Table 2 and Table 3, we see that for the snake robots locomotion the total energy required to cover a distance of 4m is less than for the ROV. For any values of the parameters of the gait pattern, both for lateral undulation and eel-like motion patterns, the underwater snake robot consumes less total energy than the remotely operated vehicle for the same task.

To conclude, the underwater snake robots consume less total energy traversing the given distance than the ROV and they are more energy efficient compare to the ROV by considering the cost of transportation as the metric. Note that the light weight and small cross-section works in favour of the energy efficiency of the snake robots. Furthermore, we see from the simulations that both systems are more energy efficient when they move at lower velocities, which was expected since the power consumption is directly connected to the achieved speed of the vehicle. However, it may be that the property that the snake robot system moves at lower velocities than the ROV contributes to making it more energy efficient. In this case, we need to pay the penalty of achieving slower motion (more time required to achieve the same travelled distance).

Based on this analysis, we see that ROVs and swimming snake robots have different advantages and can be used for different tasks. ROVs have an advantage when it comes to carrying heavy payload sensors because of their considerable size. The ROV also achieves faster motion (less time required to achieve the same travelled distance) than the snake robots. Swimming snake robots, on the other hand, are more slender and flexible structures, and thus have an advantage with respect to maneuverability and access to narrow environments. The consequences for subsea structures or divers in case of a collision are also significantly reduced compared to those of a working class ROV. In addition, the total energy consumption and the cost of transportation are significantly lower for these lightweight structures. Furthermore, for monitoring of biological systems and also other surveillance tasks, the quiet motion of the snake robots is an advantage with respect to the thruster-driven propulsion of the ROVs.

6. CONCLUSIONS AND FUTURE WORK

In this paper, we presented results regarding the power consumption of different underwater robotic systems and identified the most efficient vehicle depending on the desired motion. In

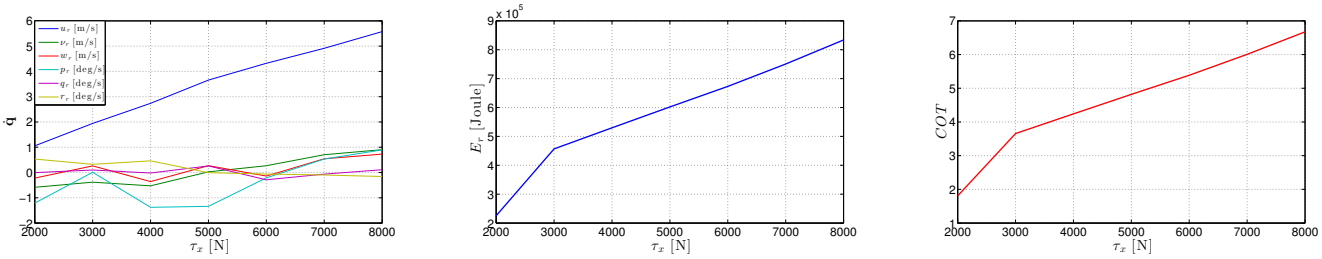

(a) Velocities of ROV (b) Total energy consumption (c) Cost of transportation

Fig. 2. Simulation results for the ROV.

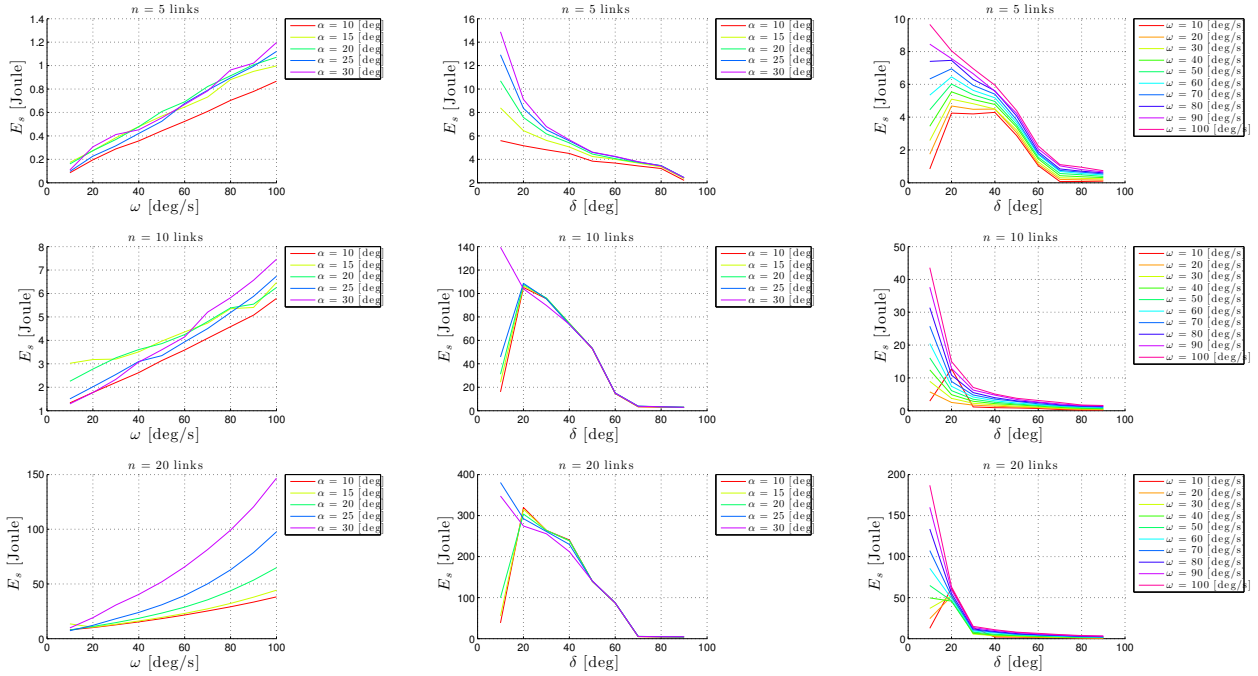

(a) For specified phase offset $\delta = 35^o,\ 15^o,\ 15^o$ (b) For constant frequency $\omega = 70^o/\text{s}$ (c) For constant amplitude $\alpha = 20^o$

Fig. 3. Total energy consumption for the lateral undulation motion pattern.

Table 2. Maximum and minimum values for the lateral undulation.

n	Max E_s	Min E_s	Max COT	Min COT
5 (Fig. 3a and Fig. 4a)	1.1967	0.1094	0.0092	$8.4544 \cdot 10^{-4}$
5 (Fig. 3b and Fig. 4b)	14.8801	2.4304	0.1150	0.0188
5 (Fig. 3c and Fig. 4c)	9.6530	0.7368	0.0746	0.0057
10 (Fig. 3a and Fig. 4a)	7.4588	1.2927	0.0288	0.0050
10 (Fig. 3b and Fig. 4b)	139.3753	2.9180	0.5384	0.0113
10 (Fig. 3c and Fig. 4c)	43.5805	1.5911	0.1684	0.0061
20 (Fig. 3a and Fig. 4a)	146.6482	9.7953	0.2833	0.0189
20 (Fig. 3b and Fig. 4b)	347.7708	4.7240	0.6717	0.0091
20 (Fig. 3c and Fig. 4c)	186.9369	3.1348	0.3611	0.0061

Table 3. Maximum and minimum values for the eel-like motion.

n	Max E_s	Min E_s	Max COT	Min COT
5 (Fig. 5a and Fig. 6a)	1.5244	0.2668	0.0118	0.0021
5 (Fig. 5b and Fig. 6b)	13.7142	3.2400	0.1060	0.0250
5 (Fig. 5c and Fig. 6c)	8.2996	0.8076	0.0641	0.0062
10 (Fig. 5a and Fig. 6a)	9.9969	3.8121	0.0386	0.0147
10 (Fig. 5b and Fig. 6b)	44.8714	3.9287	0.1733	0.0152
10 (Fig. 5c and Fig. 6c)	29.9615	1.4559	0.1157	0.0056
20 (Fig. 5a and Fig. 6a)	122.9098	15.9880	0.2374	0.0309
20 (Fig. 5b and Fig. 6b)	167.2808	5.2576	0.3231	0.0102
20 (Fig. 5c and Fig. 6c)	125.9718	2.9053	0.2433	0.0056

particular, we compared the energy efficiency of underwater snake robots with the energy efficiency of the widely used remotely operated vehicles (ROVs). A simulation study was performed comparing the total energy consumption and the cost of transportation of underwater snake robots and ROVs. Comparison results were obtained for the total energy consumption and the cost of transportation of underwater snake robots and ROVs. The simulation results showed that, both with respect to the cost of transportation metric and the total consumed energy the underwater snake robots are more energy efficient compared to the ROVs.

The results of this study should be extended further by investigating other motion patterns for underwater snake robots in order to improve even more the energy efficiency of underwater vehicles. In order to reduce even more the cost of transportation of underwater snake robots and thus increase the energy efficiency, the underwater swimming robots should adapt not only the shape and the motion patterns of biological fish but, in addition, the actuation strategies and the compliant bodies

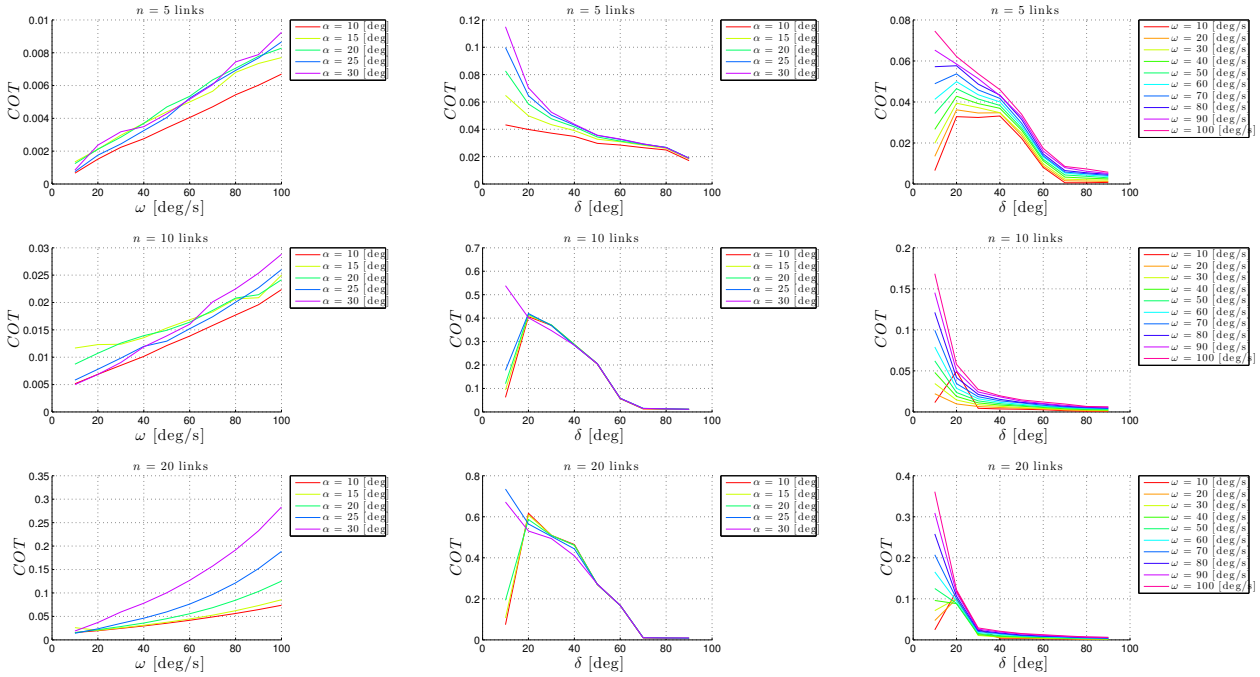

(a) For specified phase offset $\delta = 35^o,\ 15^o,\ 15^o$ (b) For constant frequency $\omega = 70^o/\text{s}$ (c) For constant amplitude $\alpha = 20^o$

Fig. 4. Cost of transportation for the lateral undulation motion pattern.

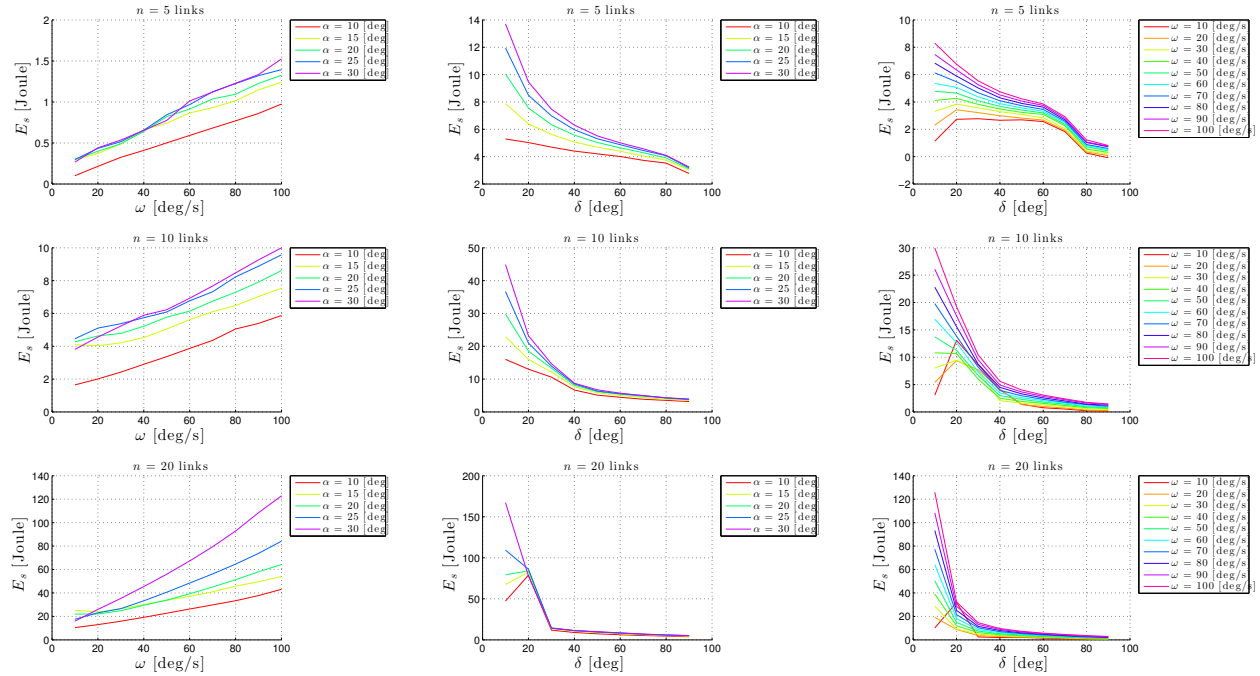

(a) For specified phase offset $\delta = [35^o\ 15^o\ 15^o]$ (b) For constant frequency $\omega = 70^o/\text{s}$ (c) For constant amplitude $\alpha = 20^o$

Fig. 5. Total energy consumption for the eel-like motion pattern.

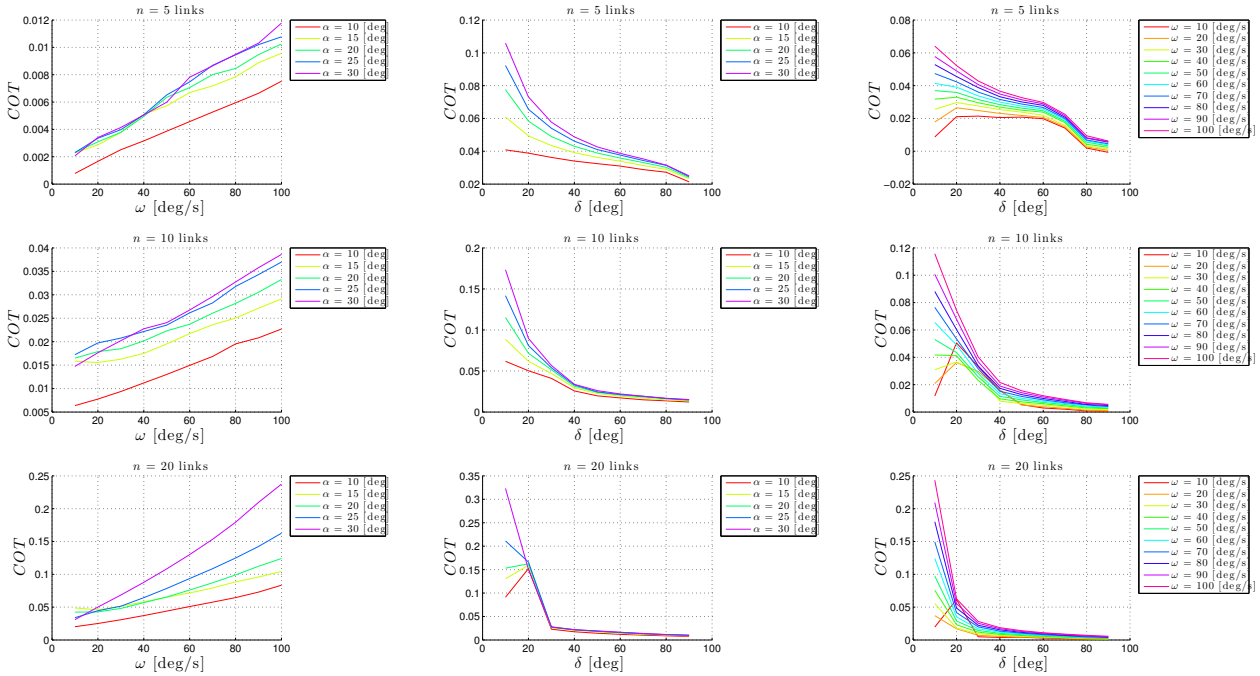

(a) For specified phase offset $\delta = [35^o\ 15^o\ 15^o]$ (b) For constant frequency $\omega = 70^o/\text{s}$ (c) For constant amplitude $\alpha = 20^o$

Fig. 6. Cost of Transportation for the eel-like motion pattern.

properties should be considered. Furthermore, in future work the authors will investigate through simulation and through experimental studies the energy efficiency of underwater snake robots compared to lightweight ROVs.

REFERENCES

Boyer, F., Porez, M., and Khalil, W. (2006). Macro-continuous computed torque algorithm for a three-dimensional eel-like robot. *IEEE Transactions on Robotics*, 22(4), 763 –775. doi: 10.1109/TRO.2006.875492.

Chen, J., Friesen, W.O., and Iwasaki, T. (2011). Mechanisms underlying rhythmic locomotion: bodyfluid interaction in undulatory swimming. *The Journal of Experimental Biology*, 214(4), 561–574. doi:10.1242/jeb.048751.

Fossen, T.I. (2011). *Handbook of Marine Craft Hydrodynamics and Motion Control*. John Wiley & Sons, Ltd. doi: 10.1002/9781119994138.ch12.

Gray, J. (1933). Studies in animal locomotion. *Journal of Experimental Biology*, 10(1), 88–104.

Guo, J. (2006). A waypoint-tracking controller for a biomimetic autonomous underwater vehicle. *Ocean Engineering*, 33, 2369 – 2380. doi: 10.1016/j.oceaneng.2005.11.012.

Hirose, S. (1993). *Biologically Inspired Robots: Snake-Like Locomotors and Manipulators*. Oxford University Press, Oxford.

Kelasidi, E., Pettersen, K.Y., and Gravdahl, J.T. (2014a). Stability analysis of underwater snake robot locomotion based on averaging theory. In *Proc. IEEE International Conference on Robotics and Biomimetics*. Bali, Indonesia.

Kelasidi, E., Pettersen, K.Y., and Gravdahl, J.T. (2015). Energy efficiency of underwater snake robot locomotion. In *Proc. 23th Mediterranean Conference on Control Automation (MED)*. (Accepted:www.dropbox.com/s/m4zmfbftcqutkv8/MED15.pdf).

Kelasidi, E., Pettersen, K.Y., Gravdahl, J.T., and Liljebäck, P. (2014b). Modeling of underwater snake robots. In *Proc. IEEE International Conference on Robotics and Automation (ICRA)*. Hong Kong, China.

Khalil, W., Gallot, G., and Boyer, F. (2007). Dynamic modeling and simulation of a 3-D serial eel-like robot. *IEEE Transactions on Systems, Man, and Cybernetics, Part C: Applications and Reviews*, 37(6), 1259 –1268. doi: 10.1109/TSMCC.2007.905831.

Liljebäck, P., Pettersen, K.Y., Stavdahl, Ø., and Gravdahl, J.T. (2013). *Snake Robots: Modelling, Mechatronics, and Control*. Springer-Verlag, Advances in Industrial Control. doi: DOI: 10.1007/978-1-4471-2996-7.

Shi, W., Stapersma, D., and Grimmelius, H. (2008). Comparison study on moving and transportation performance of transportation modes. *International journal of energy and environment*, 2.

Wiens, A. and Nahon, M. (2012). Optimally efficient swimming in hyper-redundant mechanisms: control, design, and energy recovery. *Bioinspir Biomim*, 7(4), 046016.